

https://dspace.org/

Probing anomalous couplings using di-Higgs production in electron–proton collisions

Kumar, M.; Ruan, X.; Islam, R.; Klein, M.; Klein, U. ...

2017-01
Elsevier
http://hdl.handle.net/10539/23418
Kumar, M. et al. 2017. Probing anomalous couplings using di-Higgs production in electron–proton collisions. Physics Letters B, 764 (2017), pp. 247-253

Downloaded from a DSpace repository. https://dspace.org/

Physics Letters B 764 (2017) 247–253

Contents lists available at ScienceDirect

Physics Letters B

www.elsevier.com/locate/physletb

Probing anomalous couplings using di-Higgs production in electron–proton collisions

Mukesh Kumar [a,*], Xifeng Ruan [b], Rashidul Islam [c], Alan S. Cornell [a], Max Klein [d], Uta Klein [d], Bruce Mellado [b]

[a] National Institute for Theoretical Physics, School of Physics and Mandelstam Institute for Theoretical Physics, University of the Witwatersrand, Johannesburg, Wits 2050, South Africa
[b] University of the Witwatersrand, School of Physics, Private Bag 3, Wits 2050, South Africa
[c] Department of Physics, University of Calcutta, 92, Acharya Prafulla Chandra Road, Kolkata 700009, India
[d] Oliver Lodge Laboratory, University of Liverpool, Liverpool, United Kingdom

ARTICLE INFO

Article history:
Received 25 September 2016
Received in revised form 11 November 2016
Accepted 19 November 2016
Available online 24 November 2016
Editor: G.F. Giudice

Keywords:
Higgs boson
Extensions of Higgs sector
Particle production

ABSTRACT

A proposed high energy Future Circular Hadron-Electron Collider would provide sufficient energy in a clean environment to probe di-Higgs production. Using this channel we show that the azimuthal angle correlation between the missing transverse energy and the forward jet is a very good probe for the non-standard hhh and $hhWW$ couplings. We give the exclusion limits on these couplings as a function of integrated luminosity at a 95% C.L. using the fiducial cross sections. With appropriate error fitting methodology we find that the Higgs boson self coupling could be measured to be $g^{(1)}_{hhh} = 1.00^{+0.24(0.14)}_{-0.17(0.12)}$ of its expected Standard Model value at $\sqrt{s} = 3.5(5.0)$ TeV for an ultimate 10 ab^{-1} of integrated luminosity.
© 2016 The Author(s). Published by Elsevier B.V. This is an open access article under the CC BY license (http://creativecommons.org/licenses/by/4.0/). Funded by SCOAP[3].

1. Introduction

The 125 GeV particle discovered by the ATLAS and CMS experiments [1–5] has been established as a spin-0 Higgs boson rather than a spin-2 particle [6,7]. The measurements of its couplings to fermions and gauge bosons are being updated constantly and the results confirm consistency with the expected Standard Model (SM) values [4,8–10]. However, to establish that a scalar doublet Φ does indeed break the electroweak (EW) symmetry spontaneously when it acquires a nonzero vacuum expectation value, v, requires a direct measurement of the Higgs boson self coupling, λ. The minimal SM, merely on the basis of the economy of fields and interactions, assumes the existence of only one physical scalar, h, with $J^{PC} = 0^{++}$. Although Ref. [8] has ruled out a pure pseudoscalar hypothesis at a 99.98% confidence limit (C.L.), the new particle can still have a small CP-odd admixture to its couplings.

Theoretically, the Higgs boson self coupling appears when, as a result of electroweak symmetry breaking in the SM, the scalar potential $V(\Phi)$ gives rise to the Higgs boson self interactions as follows:

$$V(\Phi) = \mu^2\Phi^\dagger\Phi + \lambda(\Phi^\dagger\Phi)^2 \rightarrow \frac{1}{2}m_h^2h^2 + \lambda v h^3 + \frac{\lambda}{4}h^4, \qquad (1)$$

where $\lambda = \lambda_{\rm SM} = m_h^2/(2v^2) \approx 0.13$ and Φ is an $SU(2)_L$ scalar doublet. For a direct and independent measurement of λ we need to access double Higgs boson production experimentally. However, this path is extremely challenging and requires a very high integrated luminosity to collect a substantial di-Higgs event rate, and an excellent detector with powerful background rejection capabilities. On the theoretical side we need to also take into account all vertices involved in the process that are sensitive to the presence of new physics beyond the SM (BSM).

There are various proposals to build new, powerful high energy e^+e^-, e^-p and pp colliders in the future. We have based our study on a *Future Circular Hadron-Electron Collider* (FCC-he) which employs the 50 TeV proton beam of a proposed 100 km circular pp collider (FCC-pp), and electrons from an Energy Recovery Linac (ERL) being developed for the *Large Hadron Electron Collider* (LHeC) [11,12]. The design of the ERL is such that the e^-p and pp colliders operate simultaneously, thus optimising the cost and the physics synergies between e^-p and pp processes. Such facilities would be potent Higgs research centres, see e.g. Ref. [13]. The LHeC and the FCC-he configuration are advantageous with respect to the Large

* Corresponding author.
E-mail addresses: mukesh.kumar@cern.ch (M. Kumar), xifeng.ruan@cern.ch (X. Ruan), rashidul.islam@cern.ch (R. Islam), alan.cornell@wits.ac.za (A.S. Cornell), Max.Klein@liverpool.ac.uk (M. Klein), Uta.Klein@liverpool.ac.uk (U. Klein), bruce.mellado.garcia@cern.ch (B. Mellado).

http://dx.doi.org/10.1016/j.physletb.2016.11.039
0370-2693/© 2016 The Author(s). Published by Elsevier B.V. This is an open access article under the CC BY license (http://creativecommons.org/licenses/by/4.0/). Funded by SCOAP[3].

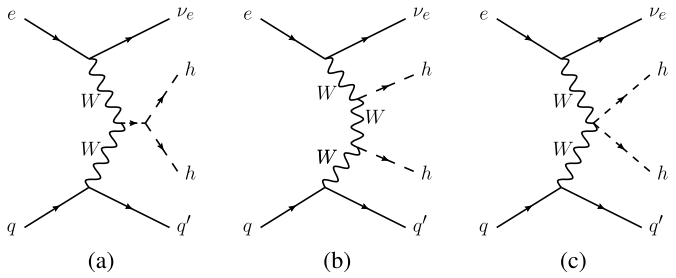


Fig. 1. Leading order diagrams contributing to the process $pe^- \to hhj\nu_e$ with $q \equiv u, c, \bar{d}, \bar{s}$ and $q' \equiv d, s, \bar{u}, \bar{c}$ respectively.

Hadron collider (LHC) (or FCC-pp in general) in terms of (1) initial states are asymmetric and hence backward and forward scattering can be disentangled, (2) it provides a clean environment with suppressed backgrounds from strong interaction processes and free from issues like pile-ups, multiple interactions etc., (3) such machines are known for high precision measurements of the dynamical properties of the proton allowing simultaneous test of EW and QCD effects. A detailed report on the physics and detector design concepts can be found in the Ref. [11].

The choice of an ERL energy of $E_e = 60$ to 120 GeV, with an available proton energy $E_p = 50\,(7)$ TeV, would provide a centre of mass (c.m.s.) energy of $\sqrt{s} \approx 3.5(1.3)$ to 5.0(1.8) TeV at the FCC-he (LHeC) using the FCC-pp (LHC) protons. The FCC-he would have sufficient c.m.s. energy to probe the Higgs boson self coupling via double Higgs boson production. The inclusive Higgs production cross section at the FCC-he is expected to be about five times larger than at the proposed 100 km circular e^+e^- collider (FCC-ee).

This article is organised as follows: We discuss the process to produce the di-Higgs events in an e^-p collider and the most general Lagrangian with all relevant new physics couplings in Section 2. In Section 3 all the simulation tools and the kinematic cuts that are required to study the sensitivity of the involved couplings are given. Here we also discuss the details of the analyses that has gone into the study. In Section 4 there is a discussion on the validity of the effective theory considered here. And finally we conclude and draw inferences from the analysis in Section 5.

2. Formalism

In an e^-p collider environment a double Higgs event can be produced through: (1) the charged current process, $pe^- \to hhj\nu_e$, and (2) the neutral current process, $pe^- \to hhje^-$, if there are no new physics processes involved. The SM background will cloud each of the processes greatly, and it will be a formidable task to separate signal from backgrounds. Here we study the charged current process because the signal strength of this is superior to the neutral current process. Hence we show in Fig. 1 the Higgs boson pair production, at leading order, due to the resonant and non-resonant contributions in charged current deep inelastic scattering (CC DIS) at an e^-p collider. As seen in Fig. 1, the di-Higgs production involves hhh, hWW and $hhWW$ couplings. Note that the hWW coupling will be extensively probed at the LHC, where its value conforms to the value predicted by the SM [4,8,10]. Through vector boson fusion Higgs production mode at the LHC, a BSM analyses to determine the CP and spin quantum numbers of the Higgs boson has been studied in Refs. [14–17]. The authors of Ref. [18] have shown the sensitivity of new physics contributions in hWW couplings at e^-p colliders through a study of the azimuthal angle correlation for single Higgs boson production in $pe^- \to hj\nu_e$ with an excellent signal-to-background ratio based on the $h \to b\bar{b}$ decay channel. Since we do not have any direct measurement of the Higgs boson self coupling (hhh) and quartic ($hhWW$) coupling, there can be several possible sources of new physics in the scalar sector. This article studies for the proposed FCC-he sensitivity of the Higgs boson self coupling around its SM value including BSM contributions by considering all possible Lorentz structures. In order to make it a complete study we also retain the possibilities for hWW couplings that appear in the di-Higgs production modes.

Following Refs. [18,19] the most general Lagrangian which can account for all bosonic couplings relevant for the phenomenology of the Higgs boson sector at the FCC-he are the three-point and four-point interactions involving at least one Higgs boson field. It can be written as:

$$\mathcal{L}^{(3)}_{hhh} = \frac{m_h^2}{2v}(1 - g^{(1)}_{hhh})h^3 + \frac{1}{2v}g^{(2)}_{hhh}h\partial_\mu h\partial^\mu h, \tag{2}$$

$$\mathcal{L}^{(3)}_{hWW} = -g\left[\frac{g^{(1)}_{hWW}}{2m_W}W^{\mu\nu}W^\dagger_{\mu\nu}h + \frac{g^{(2)}_{hWW}}{m_W}(W^\nu\partial^\mu W^\dagger_{\mu\nu}h + \text{h.c}) + \frac{\tilde{g}_{hWW}}{2m_W}W^{\mu\nu}\widetilde{W}^\dagger_{\mu\nu}h\right], \tag{3}$$

$$\mathcal{L}^{(4)}_{hhWW} = -g^2\left[\frac{g^{(1)}_{hhWW}}{4m_W^2}W^{\mu\nu}W^\dagger_{\mu\nu}h^2 + \frac{g^{(2)}_{hhWW}}{2m_W^2}(W^\nu\partial^\mu W^\dagger_{\mu\nu}h^2 + \text{h.c}) + \frac{\tilde{g}_{hhWW}}{4m_W^2}W^{\mu\nu}\widetilde{W}^\dagger_{\mu\nu}h^2\right]. \tag{4}$$

Here $g^{(i)}_{(\dots)}, i = 1, 2$, and $\tilde{g}_{(\dots)}$ are real coefficients corresponding to the CP-even and CP-odd couplings respectively (of the hhh, hWW and $hhWW$ anomalous vertices), $W_{\mu\nu} = \partial_\mu W_\nu - \partial_\nu W_\mu$ and $\widetilde{W}_{\mu\nu} = \frac{1}{2}\epsilon_{\mu\nu\rho\sigma}W^{\rho\sigma}$. In Eq. (2) $g^{(1)}_{hhh}$ is parametrised with a multiplicative constant with respect to λ_{SM} as in Eq. (1). Thus the Higgs self coupling λ appears as $g^{(1)}_{hhh}\lambda_{\text{SM}}$ in the expression for $V(\Phi)$. Clearly, in the SM $g^{(1)}_{hhh} = 1$ and all other anomalous couplings vanish in Eqs. (2)–(4). The Lorentz structures of Eqs. (2)–(4) can be derived from the $SU(2)_L \otimes U(1)_Y$ gauge invariant dimension-6 operators given in Ref. [19].

The complete Lagrangian we work with is as follows:

$$\mathcal{L} = \mathcal{L}_{\text{SM}} + \mathcal{L}^{(3)}_{hhh} + \mathcal{L}^{(3)}_{hWW} + \mathcal{L}^{(4)}_{hhWW}. \tag{5}$$

The most general effective vertices take the form:

$$\Gamma_{hhh} = -6\lambda v\left[g^{(1)}_{hhh} + \frac{g^{(2)}_{hhh}}{3m_h^2}(p_1\cdot p_2 + p_2\cdot p_3 + p_3\cdot p_1)\right], \tag{6}$$

$$\Gamma_{hW^-W^+} = gm_W\left[\left\{1 + \frac{g^{(1)}_{hWW}}{m_W^2}p_2\cdot p_3 + \frac{g^{(2)}_{hWW}}{m_W^2}(p_2^2 + p_3^2)\right\}\eta^{\mu_2\mu_3} - \frac{g^{(1)}_{hWW}}{m_W^2}p_2^{\mu_3}p_3^{\mu_2} - \frac{g^{(2)}_{hWW}}{m_W^2}(p_2^{\mu_2}p_2^{\mu_3} + p_3^{\mu_2}p_3^{\mu_3}) - \mathrm{i}\frac{\tilde{g}_{hWW}}{m_W^2}\epsilon_{\mu_2\mu_3\mu\nu}p_2^\mu p_3^\nu\right], \tag{7}$$

$$\Gamma_{hhW^-W^+} = g^2\left[\left\{\frac{1}{2} + \frac{g^{(1)}_{hhWW}}{m_W^2}p_3\cdot p_4 + \frac{g^{(2)}_{hhWW}}{m_W^2}(p_3^2 + p_4^2)\right\}\eta^{\mu_3\mu_4} - \frac{g^{(1)}_{hhWW}}{m_W^2}p_3^{\mu_4}p_4^{\mu_3} - \frac{g^{(2)}_{hhWW}}{m_W^2}(p_3^{\mu_3}p_3^{\mu_4} + p_4^{\mu_3}p_4^{\mu_4}) - \mathrm{i}\frac{\tilde{g}_{hhWW}}{m_W^2}\epsilon_{\mu_3\mu_4\mu\nu}p_3^\mu p_4^\nu\right]. \tag{8}$$

Table 1
Cross sections of signal and backgrounds in charged current (CC), neutral current (NC) and photo-production (PHOTO) modes for $E_e = 60$ GeV and $E_p = 50$ TeV, where j is light quarks and gluons. For this estimation we use basic cuts $|\eta| \leq 10$ for light-jets, leptons and b-tagged jets, $p_T \geq 10$ GeV, $\Delta R_{\min} = 0.4$ for all particles. And electron polarisation is taken to be -0.8.

Process	CC (fb)	NC (fb)	PHOTO (fb)
Signal:	2.40×10^{-1}	3.95×10^{-2}	3.30×10^{-6}
$b\bar{b}b\bar{b}j$:	8.20×10^{-1}	$3.60 \times 10^{+3}$	$2.85 \times 10^{+3}$
$b\bar{b}jjj$:	$6.50 \times 10^{+3}$	$2.50 \times 10^{+4}$	$1.94 \times 10^{+6}$
ZZj ($Z \to b\bar{b}$):	7.40×10^{-1}	1.65×10^{-2}	1.73×10^{-2}
$t\bar{t}j$ (hadronic):	3.30×10^{-1}	$1.40 \times 10^{+2}$	$3.27 \times 10^{+2}$
$t\bar{t}j$ (semi-leptonic):	1.22×10^{-1}	$4.90 \times 10^{+1}$	$1.05 \times 10^{+2}$
$hb\bar{b}j$ ($h \to b\bar{b}$):	5.20×10^{-1}	1.40×10^{0}	2.20×10^{-2}
hZj ($Z, h \to b\bar{b}$):	6.80×10^{-1}	9.83×10^{-3}	6.70×10^{-3}

The momenta and indices considered above are of the same order as they appear in the index of the respective vertex Γ. For example, in the vertex $\Gamma_{hW^-W^+}$ the momenta of h, W^- and W^+ are p_1, p_2 and p_3 respectively. Similarly, μ_2 and μ_3 are the indices of W^- and W^+. Using the above effective field theory (EFT) approach a study has been performed as an example for di-Higgs production in vector boson fusion at the LHC in Ref. [19].

3. Simulation tools and analysis

We begin our probe of the sensitivity of these couplings by building a model file for the Lagrangian in Eq. (5) using `FeynRules` [19], and then simulate the charged current double Higgs boson production channel $p e^- \to hhj\nu_e$ (see Fig. 1), with h further decaying into a $b\bar{b}$ pair,[1] in the FCC-he set up with $\sqrt{s} \approx 3.5$ TeV. Our analysis starts with optimising the SM di-Higgs signal events with respect to all possible backgrounds from multi-jet events, $ZZ +$ jets, $hb\bar{b} +$ jets, $hZ +$ jets and $t\bar{t} +$ jets in charged and neutral current deep-inelastic scattering (DIS) and in photo-production,[2] taking into account appropriate b-tagged jets and a high performance multipurpose 4π detector. In Table 1 we have given an estimation of cross sections for signal and backgrounds considering all possible modes with basic cuts. We then investigate the limits on each coupling taking BSM events as the signal. For the generation of events we use the Monte Carlo event generator `MadGraph5` [24] and the `CTEQ6L1` [25] parton distribution functions. Further fragmentation and hadronisation are done with a *customised* `Pythia-PGS`[3] [26]. The detector level simulation is performed with reasonably chosen parameters using `Delphes`[4] [27] and jets were clustered using `FastJet` [28] with the anti-k_T algorithm [29] using the distance parameter, $R = 0.4$. The factorisation and renormalisation scales for the signal simulation are fixed to the Higgs boson mass, $m_h = 125$ GeV. The background simulations are done with the default `MadGraph5` dynamic scales. The e^- polarisation is assumed to be -80%.

3.1. Cut-based optimisation

We base our simulation on the following kinematic selections in order to optimise the significance of the SM signal over all the backgrounds: (1) At least four b-tagged jets and one additional light jet are selected in an event with transverse momenta, p_T, greater than 20 GeV. (2) For *non*-b-tagged jets, the absolute value of the rapidity, $|\eta|$, is taken to be less than 7, whereas for b-tagged jets it is less than 5. (3) The four b-tagged jets must be well separated and the distance between any two jets, defined as $\Delta R = \sqrt{(\Delta\phi)^2 + (\Delta\eta)^2}$, ϕ being the azimuthal angle, is taken to be greater than 0.7. (4) Charged leptons with $p_T > 10$ GeV are rejected. (5) For the largest p_T forward jet J (the *non*-b-tagged jet after selecting at least four b-jets) $\eta_J > 4.0$ is required. (6) The missing transverse energy, $\not{E}_T$, is taken to be greater than 40 GeV. (7) The azimuthal angle between $\not{E}_T$ and the b-tagged jets are: $\Delta\Phi_{\not{E}_T,\ leading\ jet} > 0.4$ and $\Delta\Phi_{\not{E}_T,\ sub-leading\ jet} > 0.4$. (8) The four b-tagged jets are grouped into two pairs such that the distances of each pair to the true Higgs mass are minimised. The leading mass contains the leading p_T-ordered b-jet. The first pair is required to be within 95–125 GeV and the second pair within 90–125 GeV.[5] (9) The invariant mass of all four b-tagged jets has to be greater than 290 GeV.

In the selections (described above) the b-tagging efficiency is assumed to be 70%, with fake rates from c-initiated jets and light jets to the b-jets of 10% and 1% respectively. Corresponding weights[6] at a particular luminosity of 10 ab^{-1} for a signal, and all backgrounds with significance has been tabulated in Table 2. Significance at all stages of the cuts are calculated using the Poisson formula $\mathcal{S} = \sqrt{2[(S+B)\log(1+S/B) - S]}$, where S and B are the expected signal and background yields at a particular luminosity respectively.

From Table 2 we recognise that selection on the forward jet in the FCC-he type machine plays a very significant role in distinguishing the signal with respect to background. By selecting events with $\eta_J > 4.0$, there is loss of 25% of signal events, while the total background loss is around 80%. The next significant cut on missing energy ($\not{E}_T > 40$ GeV) is also very significant as due to this cut there is loss of 88% of events in total background, however, for the signal there is a loss of only 34% of events after forward jet selection. Furthermore the mass window cut for the invariant mass of two b-tagged jets, after the $\Delta\phi_{\not{E}_T j} > 0.4$ selection, significantly reduces the total background events to 5%, only while the signal events remains at 40%. Efficient requirements on the invariant mass window of four b-jets are efficient, such that to reduce backgrounds by 44% leads to a signal of 90% with respect to the previous two b-tagged jet mass window selection. And hence there is a 20% enhancement in the significance obtained in comparison to the two different mass window selection criteria, and overall with respect to initial events this cut-based optimisation is

[1] In pp collider like the LHC, the main challenge of this search is to distinguish the signal of four bottom quarks in the final state (that hadronise into jets (b-jets)) from the QCD multijet backgrounds. Such challenges and difficulties are discussed and performed in ATLAS and CMS studies [20–22].

[2] We cross checked the modelling of photo-production cross sections from `MadGraph5` by switching on the "Improved Weizsäcker–Williams approximation formula" described in Ref. [23] to give the probability of photons from the incoming electron, versus the expectation of the `Pythia` Monte Carlo generator.

[3] In `Pythia-PGS` we modified several parameters in a way to use it for e^-p collision and to get all required numbers of events demanded in each simulation. The coordinate system is set as for the HERA experiments, i.e. the proton direction defines the forward direction. The modifications have been successfully validated using neutral current DIS events and switched off QCD ISR. For e^-p collisions multiple interactions and pile-up are expected to be very small and are switched off in our studies.

[4] For `Delphes` we used the ATLAS set-up with the modifications in the $|\eta|$ ranges for forward and b-tagged jets up to 7 and 5 respectively with 70% tagging efficiency of b-jets as mentioned in the text. The resolution parameters for energy deposits in the calorimeters are based on the ATLAS Run-1 performance.

[5] Among the four b-tagged jets, choices of pairing have been performed via appropriate selection of mass window, keeping in mind to reconstruct the Higgs boson mass, m_h, in the signal as well as the Z-boson mass, m_Z, in the backgrounds. We choose the pair in which the quadratic sum $(m_1 - m_c)$ and $(m_2 - m_c)$ is smallest, and in each mass m_i, mass m_1 has the largest p_T b-jet, $m_c = (m_h - m_0)$ GeV, and normally $m_0 \approx 20$–40 GeV (which is not important, since the false pairing will have a much higher quadratic sum).

[6] Here weights mean the number of expected events at a particular luminosity. The number of events of the photo-production of $4b +$ jets are derived using the efficiencies of the Monte Carlo samples due to the low statistics. The other backgrounds are obtained directly from the event selection.

Table 2
A summary table of event selections to optimise the signal with respect to the backgrounds in terms of the weights at 10 ab^{-1}. In the first column the selection criteria are given as described in the text. The second column contains the weights of the signal process $pe^- \to hhj\nu_e$, where both the Higgs bosons decay to $b\bar{b}$ pair. In the next columns the sum of weights of all individual prominent backgrounds in charged current, neutral current and photo-production are given with each selection, whereas in the penultimate column all backgrounds' weights are added. The significance is calculated at each stage of the optimised selection criteria using the formula $\mathcal{S} = \sqrt{2[(S+B)\log(1+S/B)-S]}$, where S and B are the expected signal and background yields at a luminosity of 10 ab^{-1} respectively. This optimisation has been performed for $E_e = 60$ GeV and $E_p = 50$ TeV.

Cuts/Samples	Signal	$4b+$jets	$2b+$jets	Top	ZZ	$b\bar{b}H$	ZH	Total Bkg	Significance
Initial	2.00×10^3	3.21×10^7	2.32×10^9	7.42×10^6	7.70×10^3	1.94×10^4	6.97×10^3	2.36×10^9	0.04
At least $4b+1j$	3.11×10^2	7.08×10^4	2.56×10^4	9.87×10^3	7.00×10^2	6.32×10^2	7.23×10^2	1.08×10^5	0.94
Lepton rejection $p_T^\ell > 10$ GeV	3.11×10^2	5.95×10^4	9.94×10^3	6.44×10^3	6.92×10^2	2.26×10^2	7.16×10^2	7.75×10^4	1.12
Forward jet $\eta_J > 4.0$	233	13007.30	2151.15	307.67	381.04	46.82	503.22	16397.19	1.82
$\not{E}_T > 40$ GeV	155	963.20	129.38	85.81	342.18	19.11	388.25	1927.93	3.48
$\Delta\phi_{\not{E}_T J} > 0.4$	133	439.79	61.80	63.99	287.10	14.53	337.14	1204.35	3.76
$m^1_{bb} \in [95,125]$, $m^2_{bb} \in [90,125]$	54.5	28.69	5.89	6.68	5.14	1.42	17.41	65.23	6.04
$m_{4b} > 290$ GeV	49.2	10.98	1.74	2.90	1.39	1.21	11.01	29.23	7.51

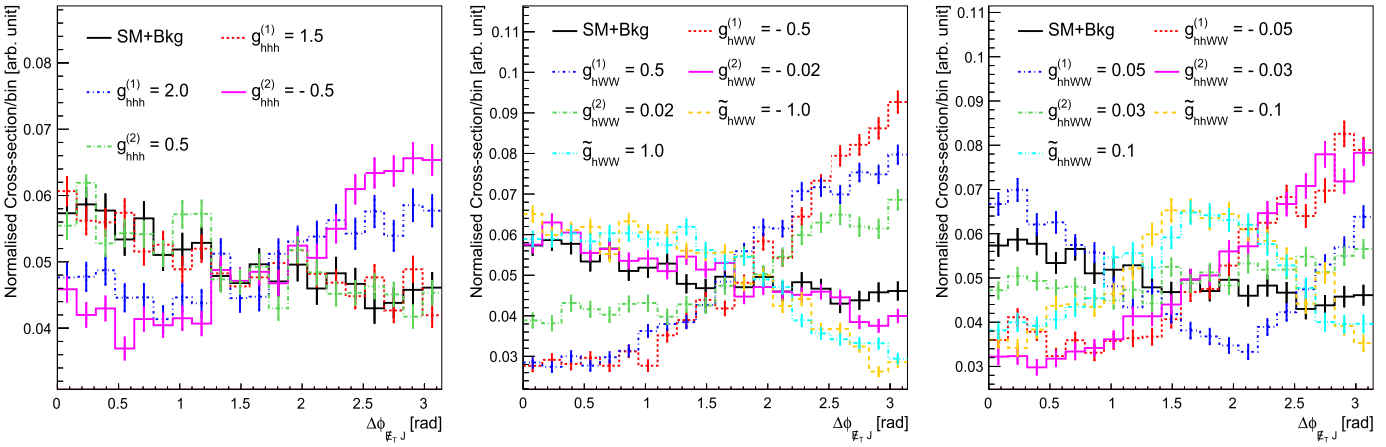


Fig. 2. Azimuthal angle distributions, at Delphes detector-level, between missing transverse energy, $\not{E}_T$, and the forward jet, J, in the SM (including backgrounds) and with the anomalous hhh, hWW and $hhWW$ couplings. The error bars are statistical.

enhanced from a 0.04 to 7.51 significance. Here it is also important to mention that photo-production of the $4b$ final state is one of the main background with similar topological final states from Zh, where $Z, h \to b\bar{b}$, and is equally important. Hence choice of efficient selection criteria is too important to reduce these backgrounds.

3.2. Kinematic distributions and observable

For our analysis we take *ad hoc* values of positive and negative couplings in such a manner that the production cross section does not deviate much from the SM value, and in particular modifications in the shapes of the normalised azimuthal angle distribution between the missing transverse energy and the leading (forward) jet are studied, in addition to other kinematic distributions.

Taking into account all the above criteria we study BSM modifications in various differential distributions at the Delphes detector-level. This leads to the following observations: (1) p_T has the usual tail behaviour, i.e. the number of events are more populated in the higher p_T region with respect to the SM for the chosen values of the anomalous couplings. (2) In cases of the η distributions: (a) For the forward jet, particularly for the couplings of hWW and $hhWW$ vertices, the mean η is more central in the detector. The behaviour is similar if we increase the c.m.s. energy of the collider by increasing E_e to higher (> 60 GeV) values. For hhh couplings the η distribution remains the same as for the SM. (b) In case of b-tagged jets, for all values of anomalous couplings, the distribution is populated around the value of η of the SM distribution. (3) For the specific observable of the azimuthal angle difference between missing transverse energy and the forward jet ($\Delta\phi_{\not{E}_T J}$) the shapes are clearly distinguishable from the SM. This behaviour is shown in Fig. 2, where the values of the couplings are *ad hoc*. However, these values are taken only for the purpose of illustration, and in the limit of the couplings going to their SM values the shapes will coincide with the SM distributions. The specific characteristics of the curves also depend on the details of the selection requirements, but the qualitative differences could be seen at every selection step. The shape of the curves is due to the fact that all new physics couplings have a momentum dependent structure (apart from $g^{(1)}_{hhh}$) and positive or negative interference with SM events. We note that $\Delta\phi_{\not{E}_T J}$ is a novel observable and commands more focused and deeper analyses. In this regard one should follow the analysis (as performed in Ref. [30]) based on an asymmetry with two equal bins in $\Delta\phi_{\not{E}_T J} \lessgtr \pi/2$, defined as

$$\mathcal{A}_{\Delta\phi_{\not{E}_T J}} = \frac{|A_{\Delta\phi>\pi/2}| - |A_{\Delta\phi<\pi/2}|}{|A_{\Delta\phi>\pi/2}| + |A_{\Delta\phi<\pi/2}|}, \tag{9}$$

in which A is the yields obtained for the given ab^{-1} data after all of the selections, including both the signal and backgrounds. Table 3 shows the estimation of the asymmetry for a set of representative values of the couplings, shown in Fig. 2, along with the associated statistical uncertainty. Though the new physics couplings are representative, we can infer the sensitivities of these couplings with respect to the SM+Bkg estimation of asymmetry from Table 3, where $g^{(1)}_{hWW}$ seems to have large fluctuations for both positive and negative choices of its values. Similarly the sensitivities of $g^{(2)}_{hhWW}$ and $\tilde{g}_{hhWW}$ can also be noted, however $g^{(1)}_{hhWW}$ is more sensible for the negative choice of its value. The study of the sensitivity of the non-standard couplings through this asym-

Table 3
Estimation of the asymmetry, defined in Eq. (9), and statistical error associated with the kinematic distributions in Fig. 2 at an integrated luminosity of 10 ab^{-1}. The cross section (σ) for the corresponding coupling choice is given in the last column with same parameters as in Table 1.

Samples		$\mathcal{A}_{\Delta\phi_{\not{E}_T j}}$	σ (fb)
SM+Bkg		0.277 ± 0.088	
$g^{(1)}_{hhh}$	$= 1.5$	0.279 ± 0.052	0.18
	$= 2.0$	0.350 ± 0.053	0.21
$g^{(2)}_{hhh}$	$= -0.5$	0.381 ± 0.050	0.19
	$= 0.5$	0.274 ± 0.024	0.74
$g^{(1)}_{hWW}$	$= -0.5$	0.506 ± 0.022	0.88
	$= 0.5$	0.493 ± 0.020	0.94
$g^{(2)}_{hWW}$	$= -0.02$	0.257 ± 0.025	0.67
	$= 0.02$	0.399 ± 0.040	0.33
$\tilde{g}_{hWW}$	$= -1.0$	0.219 ± 0.016	1.53
	$= 1.0$	0.228 ± 0.016	1.53
$g^{(1)}_{hhWW}$	$= -0.05$	0.450 ± 0.033	0.52
	$= 0.05$	0.254 ± 0.029	0.68
$g^{(2)}_{hhWW}$	$= -0.03$	0.462 ± 0.022	1.22
	$= 0.03$	0.333 ± 0.018	1.46
$\tilde{g}_{hhWW}$	$= -0.1$	0.351 ± 0.020	1.60
	$= 0.1$	0.345 ± 0.020	1.61

metry observable considering a kinematic distribution is basically corresponding to two bins by dividing the whole distribution in two halves with large bin-width. Moreover, this kind of study can be further appended with finer bin widths and a more efficient χ^2 analysis (for example in Ref. [30]). However, these detailed analyses are beyond the scope of this article.

3.3. Exclusion limits through fiducial cross section as a function of luminosity

Furthermore, we probe the exclusion limits on these couplings as a function of the integrated luminosity, with the log-likelihood method described in Ref. [31], using directly the fiducial inclusive cross section as an observable. In Fig. 3 we present exclusion plots at 95% C.L. for anomalous hhh, hWW and $hhWW$ couplings, where the shaded areas are the allowed region. The exclusion limits are based on the SM 'di-Higgs signal + backgrounds' hypotheses considering BSM contributions as the signal at the given luminosity. Each limit is given by scanning one coupling and fixing the other couplings to their SM value, where a 5% systematic uncertainty is taken into account on the signal and background yields respectively. From Fig. 3 our observations are as follows: (1) If the integrated luminosity exceeds 0.5 ab^{-1} $g^{(1)}_{hhh}$ is restricted to be positive. $g^{(1)}_{hhh}$ is allowed to be within 0.7–2.5 when the integrated luminosity reaches 15 ab^{-1} as for values of $1 < g^{(1)}_{hhh} \leq 2.1$ the cross section is smaller than the SM di-Higgs production. (2) The $g^{(2)}_{hhh}$ value is restricted to around 10^{-1}. We only exclude the positive part of this coupling because its negative part has cancellations with the SM di-Higgs cross section. (3) The sensitivity for hWW couplings, namely $g^{(1)}_{hWW}$ and $\tilde{g}_{hWW}$, can be better probed at much lower energies and luminosity at the LHeC using the single Higgs boson production as shown in Ref. [18]. However, we have shown the sensitivity of $g^{(2)}_{hWW}$, which is not considered in Ref. [18], and it is of the order 10^{-2} in the allowed region. (4) One important aspect of di-Higgs production in this type of collider is that one can measure the sensitivity of the $hhWW$ couplings also. In our analysis, since the CP-even (odd) coupling $g^{(1)}_{hhWW}$ ($\tilde{g}_{hhWW}$) has similar Lorentz structures, with the sensitivity of the exclusion plot having almost the same order of magnitude. However, the structure

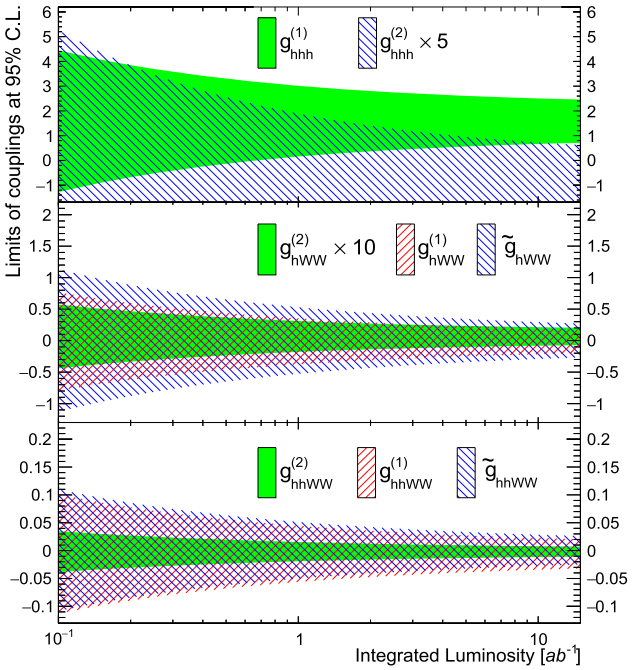


Fig. 3. The exclusion limits on the anomalous hhh (top panel), hWW (middle panel) and $hhWW$ (lower panel) couplings at 95% C.L. as a function of integrated luminosity (shaded areas). Note that the allowed values of $g^{(2)}_{hhh}$ and $g^{(2)}_{hWW}$ are multiplied by 5 and 10 respectively to highlight their exclusion region, since the values are of the order 10^{-1}.

of $g^{(2)}_{hhWW}$ allows a comparatively narrower region of values. The couplings belonging to both the hWW and $hhWW$ vertices are strongly constrained because of their high production cross section at very low values of the couplings. By increasing the luminosity from 0.1–1 ab^{-1} the constraint on the couplings increases and its limits are reduced by a factor two. A further increase of the luminosity will not change the results. All limits are derived by varying only one coupling at a time, as mentioned earlier. The exclusion limits on the couplings in this analysis are based on the constraints from an excess above the SM expectation while potential deficits from interference contributions are not sensitive yet to be used for limit settings.

3.4. Prospects at higher E_e and sensitivity of the Higgs self coupling

Finally we discuss what happens once the electron energy E_e is increased to higher values, where we focus our analysis on a determination of the SM Higgs self coupling, assuming no further BSM contributions. Without going into detail we can note that with increasing E_e (from 60 GeV to 120 GeV) the SM signal and dominant background production cross sections are enhanced by a factor of 2.2 and 2.1 respectively. As a result, the cut efficiency for the selection of four b-tagged jets and one forward jet is improved, but for the other cuts described previously (invariant mass, $\not{E}_T$, η_J and $\Delta\phi_{\not{E}_T j}$) it remains very similar. This leads to an enhancement of the selected signal and dominant background events by a factor 2.5 and 2.6 respectively. Hence we would obtain the same statistical precision with only 40% of the luminosity of an $E_e = 60$ GeV beam when increasing the electron energy to 120 GeV. At an ultimate integrated luminosity of 10 ab^{-1}, increasing E_e from 60 to 120 GeV would increase the significance of the observed SM di-Higgs events from 7.2 to 10.6, obtained from a log-likelihood fit. This includes a 5% signal and background systematics mentioned earlier. For the SM Higgs boson self coupling, where the scaling factor is expected to be $g^{(1)}_{hhh} = 1$, we perform an intelligent signal

injection test, which gives locally measured uncertainties for $g^{(1)}_{hhh}$. From this test the 1σ error band around the expected SM strength of this coupling is $g^{(1)}_{hhh} = 1.00^{+0.24(0.14)}_{-0.17(0.12)}$ for $E_e = 60(120)$ GeV.

4. Validity of EFT

In the EFT-based approach for our analyses, the usual SM Lagrangian is supplemented by higher-dimensional operators that parametrise the possible effects of new states assumed to appear at energies larger than the effective scales identified with m_W (or equivalently v) by restricting the operators of dimension less than or equal to six. We have estimated the sensitivity of the involved coupling coefficients appearing in the effective Lagrangians in Eqs. (2)–(4) with the EW scale for the derivative terms. A detailed discussion with general couplings and mass scales with a higher dimension EFT Lagrangian can be found in Ref. [32]. For the processes at high energy, it is well known that an EFT approach provides an accurate description of the underlying new physics as long as the energies are below the new physics scale, Λ, and thus the limits on the couplings obtained in the above analyses shall degrade at scales higher than the EW scales (since for the fixed values of the couplings, the interference and pure BSM terms always give low contributions in the cross section measurements for high values of scale choice). Also for $\mathcal{O}(1)$ values of anomalous couplings (apart from $g^{(1)}_{hhh}$) $g^{(i)}_{(\cdots)}$, $\tilde{g}_{(\cdots)}$ and TeV-scale momenta, one reaches the regime where the operators in Eqs. (2)–(4) may not be dominant, and operators with four and more derivatives may be equally important. In other words, the EFT behind these Lagrangian expansions breaks down. It would be important then to know how much the projected sensitivity depends on events that violate this EFT bound. With an EW precision test in Ref. [33], it is shown how an EFT's reach deteriorates when only data below the cutoff scales are employed on the mass variable in the case of Drell–Yan processes at the LHC.

A similar exercise can be performed in our case to estimate the deterioration of limits on anomalous tensorial couplings $g^{(i)}_{(\cdots)}$ and $\tilde{g}_{(\cdots)}$ (the coupling coefficients which corresponds to momentum-dependent Lorentz structure) as a function of the cut-off scale. In this approach we put an upper cut on the di-Higgs invariant mass (m'_{4b})[7] such that EFT-violating events ($> m'_{4b}$) are cut away, and then we estimate by how much the projected sensitivity of $g^{(2)}_{hhh}$, $g^{(1,2)}_{hWW}$, $g^{(1,2)}_{hhWW}$ and $\tilde{g}_{hWW}$, $\tilde{g}_{hhWW}$ degrades with respect to their previous limits. In Fig. 4 we present the percentage of deterioration of the exclusion limits of these anomalous effective couplings by selecting events below $m'_{4b} \in [0.35, 1]$ TeV for fixed luminosity of 1 ab^{-1} and 10 ab^{-1} at 95% C.L. It is apparent from Fig. 4 that the deterioration in the limits of these anomalous couplings is large for low values of the m'_{4b} cut, because the effective cross section decreases (which is equivalent to the increase of the scale Λ of the tensorial couplings) with the decrease of the values of m'_{4b}. Comparing the exclusion limits obtained in Fig. 3 we observed that at $m'_{4b} = 350$ GeV the percentage of deterioration in $g^{(2)}_{hhh}$ is more than 100%, while other hWW and $hhWW$ couplings deteriorate by 60–80% on both upper and lower sides at 1 ab^{-1} and 10 ab^{-1}. After 350 GeV a sudden decrease in degradation percentage can be noticed for $m'_{4b} = 400$–450 GeV for all couplings. Furthermore

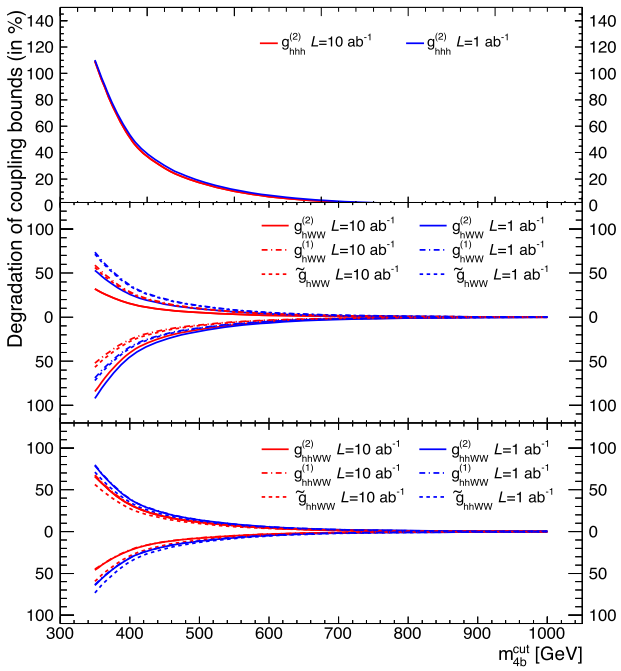


Fig. 4. Percentage of deterioration of exclusion limits of anomalous tensorial couplings (shown in Fig. 3) with respect to the upper di-Higgs invariant mass cut $m'_{4b} \equiv m^{cut}_{4b}$ [in GeV] for fixed luminosity of 1 ab^{-1} (*blue*) and 10 ab^{-1} (*red*). The numbers in the vertical axis above (below) 0 is the degradation in the upper (lower) limits. (For interpretation of the references to colour in this figure legend, the reader is referred to the web version of this article.)

around 500 GeV for $g^{(2)}_{hhh}$, it remains 18% while others are around 10%. Beyond a 650 GeV cut, all the couplings converge to the original value of limits obtained in our previous analyses, as shown in Fig. 3.

5. Summary and conclusions

We conclude that the FCC-he, with an ERL energy of $E_e \geq 60$ GeV and a proton energy $E_p = 50$ TeV, would provide significant di-Higgs event rates, and through this channel one can probe accurately the Higgs boson self coupling provided that integrated luminosities of more than 1 ab^{-1} may be achieved. Along with the Higgs self coupling one can search for any BSM signal through the measurement of the anomalous $hhWW$ contributions. One interesting feature of this type of machine is recognised by identifying forward jets in the signal events where an appropriate selection, as shown for our study, reduces backgrounds efficiently around 80% with a loss of only 25% of signal events. Our work also shows that $\Delta\phi_{\not{E}_T j}$ is a very good observable for any new physics contributions in the given channel. Estimation of an asymmetry observable in $\Delta\phi_{\not{E}_T j}$ for this kinematic distribution gives a preliminary idea of sensitivities of any new non-standard couplings. The limits on each coupling are set by measuring the observed event rate. But the asymmetry in $\Delta\phi_{\not{E}_T j}$ can provide more distinguishability of the new physics, especially cancelling many potential systematics, which is helpful to distinguish the signatures of each model. An exclusion limit with respect to luminosity for these couplings is studied, and a signal injection test shows the uncertainty of the Higgs self coupling around its expected SM strength.

With all these analyses we infer that the order of sensitivities of all non-standard couplings considered for our study within most of the luminosity ranges are consistent with the adopted methodology of asymmetry observable, and exclusion limits through fiducial cross sections at 95% C.L. However, at luminosities ∼10–15 ab^{-1}

[7] Note that in previous subsections we used the notation m_{4b} for the lowest cut on di-Higgs invariant mass. Here we use m'_{4b} to avoid confusion since for all analyses apart from the EFT validity we selected the events $m_{4b} > 290$ GeV to suppress backgrounds and increase the overall significance. Here, to investigate the sensitivity of BSM tensorial couplings, we chose the events below m'_{4b} cuts, keeping $m_{4b} > 290$ GeV so that an one to one comparison can be performed.

or higher, the method based on fiducial cross sections constrains the non-standard couplings more tightly. In addition to the fiducial cross sections, the drastic change in $\Delta\phi_{\not{E}_T j}$ shape for $g^{(1)}_{hhh}$ around 2.0 with respect to the SM in Fig. 2 (left), suggest that using further observables like $\Delta\phi_{\not{E}_T j}$ may significantly improve the sensitivity of BSM couplings in general. It is to be noted that the non-standard momentum dependent structures of the EFT breaks down at the TeV energy regime for couplings of $\mathcal{O}(1)$ and then additional derivative terms become relevant. Hence we also show the deteriorations in the limits of anomalous tensorial couplings for different regions of di-Higgs invariant mass (upper) cuts by an exclusion at fixed luminosity of 1 ab^{-1} and 10 ab^{-1} corresponding to 95% C.L. limits, with respect to the limits obtained using fiducial inclusive cross section as an observable. This method is used as an alternative approach to estimate the sensitivity of the scale dependent couplings in EFT and gives a probe to understand the regions where validity of EFT breaks down.

Our studies show a unique capability and potential of FCC-he collider to probe the precision measurement of not only the Higgs boson self coupling but also other involved couplings with tensorial structure through di-Higgs boson production.

Acknowledgements

We acknowledge fruitful discussions within the LHeC Higgs group, especially with Masahiro Kuze and Masahiro Tanaka. RI acknowledges the DST-SERB grant SRIS2/HEP-13/2012 for partial financial support.

References

[1] G. Aad, et al., Observation of a new particle in the search for the standard model Higgs boson with the ATLAS detector at the LHC, Phys. Lett. B 716 (2012) 1–29, http://dx.doi.org/10.1016/j.physletb.2012.08.020, arXiv:1207.7214.

[2] S. Chatrchyan, et al., Observation of a new boson at a mass of 125 GeV with the CMS experiment at the LHC, Phys. Lett. B 716 (2012) 30–61, http://dx.doi.org/10.1016/j.physletb.2012.08.021, arXiv:1207.7235.

[3] G. Aad, et al., Measurement of the Higgs boson mass from the $H \to \gamma\gamma$ and $H \to ZZ^* \to 4\ell$ channels with the ATLAS detector using 25 fb^{-1} of pp collision data, Phys. Rev. D 90 (5) (2014) 052004, http://dx.doi.org/10.1103/PhysRevD.90.052004, arXiv:1406.3827.

[4] V. Khachatryan, et al., Precise determination of the mass of the Higgs boson and tests of compatibility of its couplings with the standard model predictions using proton collisions at 7 and 8 TeV, Eur. Phys. J. C 75 (5) (2015) 212, http://dx.doi.org/10.1140/epjc/s10052-015-3351-7, arXiv:1412.8662.

[5] G. Aad, et al., Combined measurement of the Higgs boson mass in pp collisions at $\sqrt{s} = 7$ and 8 TeV with the ATLAS and CMS experiments, Phys. Rev. Lett. 114 (2015) 191803, http://dx.doi.org/10.1103/PhysRevLett.114.191803, arXiv:1503.07589.

[6] S. Chatrchyan, et al., Study of the mass and spin-parity of the Higgs boson candidate via its decays to Z boson pairs, Phys. Rev. Lett. 110 (8) (2013) 081803, http://dx.doi.org/10.1103/PhysRevLett.110.081803, arXiv:1212.6639.

[7] G. Aad, et al., Evidence for the spin-0 nature of the Higgs boson using ATLAS data, Phys. Lett. B 726 (2013) 120–144, http://dx.doi.org/10.1016/j.physletb.2013.08.026, arXiv:1307.1432.

[8] V. Khachatryan, et al., Constraints on the spin-parity and anomalous HVV couplings of the Higgs boson in proton collisions at 7 and 8 TeV, Phys. Rev. D 92 (1) (2015) 012004, http://dx.doi.org/10.1103/PhysRevD.92.012004, arXiv:1411.3441.

[9] G. Aad, et al., Study of the spin and parity of the Higgs boson in diboson decays with the ATLAS detector, Eur. Phys. J. C 75 (10) (2015) 476, http://dx.doi.org/10.1140/epjc/s10052-015-3685-1, Erratum: Eur. Phys. J. C 76 (3) (2016) 152, http://dx.doi.org/10.1140/epjc/s10052-016-3934-y, arXiv:1506.05669.

[10] G. Aad, et al., Measurements of the Higgs boson production and decay rates and coupling strengths using pp collision data at $\sqrt{s} = 7$ and 8 TeV in the ATLAS experiment, Eur. Phys. J. C 76 (1) (2016) 6, http://dx.doi.org/10.1140/epjc/s10052-015-3769-y, arXiv:1507.04548.

[11] J.L. Abelleira Fernandez, et al., A large hadron electron collider at CERN: report on the physics and design concepts for machine and detector, J. Phys. G 39 (2012) 075001, http://dx.doi.org/10.1088/0954-3899/39/7/075001, arXiv:1206.2913.

[12] O. Bruening, M. Klein, The large hadron electron collider, Mod. Phys. Lett. A 28 (16) (2013) 1330011, http://dx.doi.org/10.1142/S0217732313300115, arXiv:1305.2090.

[13] J.L. Abelleira Fernandez, et al., On the relation of the LHeC and the LHC, arXiv:1211.5102.

[14] T. Plehn, D.L. Rainwater, D. Zeppenfeld, Determining the structure of Higgs couplings at the LHC, Phys. Rev. Lett. 88 (2002) 051801, http://dx.doi.org/10.1103/PhysRevLett.88.051801, arXiv:hep-ph/0105325.

[15] K. Hagiwara, Q. Li, K. Mawatari, Jet angular correlation in vector-boson fusion processes at hadron colliders, J. High Energy Phys. 07 (2009) 101, http://dx.doi.org/10.1088/1126-6708/2009/07/101, arXiv:0905.4314.

[16] A. Djouadi, R.M. Godbole, B. Mellado, K. Mohan, Probing the spin-parity of the Higgs boson via jet kinematics in vector boson fusion, Phys. Lett. B 723 (2013) 307–313, http://dx.doi.org/10.1016/j.physletb.2013.04.060, arXiv:1301.4965.

[17] C. Englert, D. Goncalves-Netto, K. Mawatari, T. Plehn, Higgs quantum numbers in weak boson fusion, J. High Energy Phys. 01 (2013) 148, http://dx.doi.org/10.1007/JHEP01(2013)148, arXiv:1212.0843.

[18] S.S. Biswal, R.M. Godbole, B. Mellado, S. Raychaudhuri, Azimuthal angle probe of anomalous HWW couplings at a high energy ep collider, Phys. Rev. Lett. 109 (2012) 261801, http://dx.doi.org/10.1103/PhysRevLett.109.261801, arXiv:1203.6285.

[19] A. Alloul, B. Fuks, V. Sanz, Phenomenology of the Higgs effective Lagrangian via FEYNRULES, J. High Energy Phys. 04 (2014) 110, http://dx.doi.org/10.1007/JHEP04(2014)110, arXiv:1310.5150.

[20] G. Aad, et al., Search for Higgs boson pair production in the $b\bar{b}b\bar{b}$ final state from pp collisions at $\sqrt{s} = 8$ TeV with the ATLAS detector, Eur. Phys. J. C 75 (9) (2015) 412, http://dx.doi.org/10.1140/epjc/s10052-015-3628-x, arXiv:1506.00285.

[21] G. Aad, et al., Searches for Higgs boson pair production in the $hh \to bb\tau\tau, \gamma\gamma WW^*, \gamma\gamma bb, bbbb$ channels with the ATLAS detector, Phys. Rev. D 92 (2015) 092004, http://dx.doi.org/10.1103/PhysRevD.92.092004, arXiv:1509.04670.

[22] V. Khachatryan, et al., Search for resonant pair production of Higgs bosons decaying to two bottom quark antiquark pairs in proton proton collisions at 8 TeV, Phys. Lett. B 749 (2015) 560–582, http://dx.doi.org/10.1016/j.physletb.2015.08.047, arXiv:1503.04114.

[23] V.M. Budnev, I.F. Ginzburg, G.V. Meledin, V.G. Serbo, The two photon particle production mechanism. Physical problems. Applications. Equivalent photon approximation, Phys. Rep. 15 (1975) 181–281, http://dx.doi.org/10.1016/0370-1573(75)90009-5.

[24] J. Alwall, M. Herquet, F. Maltoni, O. Mattelaer, T. Stelzer, MadGraph 5: going beyond, J. High Energy Phys. 06 (2011) 128, http://dx.doi.org/10.1007/JHEP06(2011)128, arXiv:1106.0522.

[25] J. Pumplin, D.R. Stump, J. Huston, H.L. Lai, P.M. Nadolsky, W.K. Tung, New generation of parton distributions with uncertainties from global QCD analysis, J. High Energy Phys. 07 (2002) 012, http://dx.doi.org/10.1088/1126-6708/2002/07/012, arXiv:hep-ph/0201195.

[26] T. Sjostrand, S. Mrenna, P.Z. Skands, PYTHIA 6.4 physics and manual, J. High Energy Phys. 05 (2006) 026, http://dx.doi.org/10.1088/1126-6708/2006/05/026, arXiv:hep-ph/0603175.

[27] J. de Favereau, C. Delaere, P. Demin, A. Giammanco, V. Lemaître, A. Mertens, M. Selvaggi, DELPHES 3, a modular framework for fast simulation of a generic collider experiment, J. High Energy Phys. 02 (2014) 057, http://dx.doi.org/10.1007/JHEP02(2014)057, arXiv:1307.6346.

[28] M. Cacciari, G.P. Salam, G. Soyez, FastJet user manual, Eur. Phys. J. C 72 (2012) 1896, http://dx.doi.org/10.1140/epjc/s10052-012-1896-2, arXiv:1111.6097.

[29] M. Cacciari, G.P. Salam, G. Soyez, The Anti-k(t) jet clustering algorithm, J. High Energy Phys. 04 (2008) 063, http://dx.doi.org/10.1088/1126-6708/2008/04/063, arXiv:0802.1189.

[30] S. Dutta, A. Goyal, M. Kumar, B. Mellado, Measuring anomalous Wtb couplings at e^-p collider, Eur. Phys. J. C 75 (12) (2015) 577, http://dx.doi.org/10.1140/epjc/s10052-015-3776-z, arXiv:1307.1688.

[31] G. Cowan, K. Cranmer, E. Gross, O. Vitells, Asymptotic formulae for likelihood-based tests of new physics, Eur. Phys. J. C 71 (2011) 1554, http://dx.doi.org/10.1140/epjc/s10052-011-1554-0, Erratum: Eur. Phys. J. C 73 (2013) 2501, http://dx.doi.org/10.1140/epjc/s10052-013-2501-z, arXiv:1007.1727.

[32] G.F. Giudice, C. Grojean, A. Pomarol, R. Rattazzi, The strongly-interacting light Higgs, J. High Energy Phys. 06 (2007) 045, http://dx.doi.org/10.1088/1126-6708/2007/06/045, arXiv:hep-ph/0703164.

[33] M. Farina, G. Panico, D. Pappadopulo, J.T. Ruderman, R. Torre, A. Wulzer, Energy helps accuracy: electroweak precision tests at hadron colliders, arXiv:1609.08157.